Hindawi
Journal of Robotics
Volume 2017, Article ID 2423643, 20 pages
https://doi.org/10.1155/2017/2423643

Research Article

Bounded Control of an Actuated Lower-Limb Exoskeleton

Michael Oluwatosin Ajayi,[1,2] Karim Djouani,[1,2] and Yskandar Hamam[1,3]

[1]*F'SATI, Department of Electrical Engineering, Tshwane University of Technology, Staatsartillerie Road, Pretoria West, Pretoria, South Africa*
[2]*LISSI, University of Paris Est Creteil (UPEC), 94400 Vitry Sur Seine, France*
[3]*LISV, Bâtiment Boucher, Pole Scientifique et Technologique de Vélizy, 10-12 avenue de l'Europe, 78140 Vélizy, France*

Correspondence should be addressed to Michael Oluwatosin Ajayi; ajayimo@tut.ac.za

Received 20 June 2017; Accepted 24 September 2017; Published 3 December 2017

Academic Editor: Gordon R. Pennock

A bounded control strategy is employed for the rehabilitation and assistance of a patient with lower-limb disorder. Complete and partial lower-limb motor function disorders are considered. This application is centered on the knee and the ankle joint level, thereby considering a user in a sitting position. A high gain observer is used in the estimation of the angular position and angular velocities which is then applied to the estimation of the joint torques. The level of human contribution is feedback of a fraction of the estimated joint torque. This is utilised in order to meet the demands for a bounded human torque; that is, $\tau_h \leq N_{2,n} \leq N_{1,n}$. The asymptotic stability of the bounded control law without human contribution and the convergence analysis of the high gain observer is verified using Lyapunov-based analysis. Simulations are performed to verify the proposed control law. Results obtained guarantee a fair trajectory tracking of the physiotherapist trajectory.

1. Introduction

Wearable robots such as exoskeletons fall into a class of robot manipulators. However, they have to be worn by humans for the purpose of enhancing their movement. One of the interesting features of wearable robots is the fact that they enable healthy wearers to perform stressful activities easily over a lengthy period of time. This sole attribute has made their use in the domain of rehabilitation and assistance quite appreciated, with an extension to the medical, military, and agricultural field. Wearable exoskeletons are electromechanical devices driven by actuators in order to induce the movement of the embodied limbs. In the process of inducing this movement, there remains a possibility of human torque contribution via these limbs through the activities of the muscles, thus delivering part of the torque during rehabilitation.

In the near future, it is envisaged that the number of elderly people in world population will increase considerably; therefore this will further increase the burden of treating the health risks associated with aging by physiotherapists [1]. Robotic therapy solutions that give rise to the use of intelligent machines that are capable of offering solutions that promote motor recovery and better understanding of motor control [2, 3] remain the only efficient way to alleviate physiotherapists from this time and energy consuming exercise; thereby reducing the demands on these assist practitioners [4]. Certainly, the goal of robotic therapy is to assist in a way by automating the performance of repetitive motor-therapy for humans [5]. Robotic solutions could be either assistive, rehabilitative, or both, depending on the purpose of the design. However, the conceptual design with regard to performance-augmenting applications is always based on maintaining the human-exoskeleton kinematic compatibility [6]. This was addressed in [7]; nevertheless, for the purpose of simplicity, in this work, human-exoskeleton misalignment is not considered, and the human-exoskeleton joint axes are assumed to align. In addition, the development of active exoskeletons determines its future and some eventual activities associated with the rehabilitation systems in conjunction with expanding its working capabilities with humans [8].

In rehabilitative robotics, the solutions developed are aimed at optimising existing therapeutic approaches in order to improve or cure motor lost functions after a disabling

encounter. Assistive robotics provides solutions that will assist and interact with individuals with reduced motor functionalities so as to help them increase their self-reliance and in sustaining a fulfilling lifestyle within their personal environment [9]. Nevertheless, there exist technical similarities between them, in that the primary subject of interest is centered on the motor performance of the patient.

Utilising robotic systems for assistance and rehabilitation, the wearer could be passive or active throughout the whole session of training. When passive, the wearer voluntary movement tends to be limited since the lower-limb rehabilitation device is only designed to assist the user to follow predefined movement patterns with the aid of certain control methods. Although this method has been proven to be an effective therapeutic measure [10, 11], the need for patients to be actively involved in robotic therapy brings about more success in the results obtained [12]. One rehabilitative method which further validates this proof is the "assist-as-needed" paradigm [13, 14]. Kong and Tomizuka in [15] also designed a rehabilitation device connected to the human via elastic components which are meant to assist the human by generating assistive force to enable the human lower limbs to follow the motion of the links. Most especially, the need to ensure the safety of the wearer is essential as highlighted in [16].

Often the contribution of the wearers may be determined using on-board sensors such as EMG, Electroencephalogram (EEG), Inertial Measurement Unit (IMU), camera, and adequate algorithms to detect and classify the intention. Electromyography (EMG) control strategy is one that promotes the user specific support for controllers by converting EMG signals into desired human torques which is then partly applied by the exoskeleton device [17, 18]. However, this method is somewhat sensitive to noise and sensor location [19].

Furthermore, it is required that since wearable exoskeletons fall into the category of robot manipulators which require control input constraints, the need for the use of a bounded control law is paramount. Controllers used for exoskeletons also need to be robust enough against uncertainties [20] of which the bounded control may be a perfect fit. Bounded control literally refers to the control of a system within certain bounded variables. This type of control method seeks to define certain limits that correspond to the physical limit of the variable in question and therefore consequently helps minimize the power requirements for actuating the exoskeleton [21]. The variables often considered are those of the amplitude of the actuators. This is to avoid the possibility of an irreversible damage to the actuator [22, 23]. An in-depth description of this control method is given in [24]. In [25, 26] the authors propose a bounded control method based on nested saturations for the rehabilitation of the knee joint and a full exoskeleton with four degrees of freedom, respectively. By "nested saturation" it is meant that the actuator is subjected to magnitude and rate saturation simultaneously [27]. This not only allows maintaining the bounded inputs of the control torque, but also provides an efficient convergence of the position and velocity of the physical system. In [28], an adaptive observer-based controller for an upper-limb exoskeleton robot is proposed and the boundedness is also proven.

Due to increased use of wearable robots, which is basically inclined towards providing support to humans to effectively perform their daily activities, the force control has continued to attract the attention of many researchers. The force sensors have been often used; however this makes the system bulky and costly. Hence, the use of encoders to obtain the information external force has been exploited in [29, 30]. In [31] an observer-based user torque estimation is also used to evaluate the patient-active rehabilitation task in order to avoid the use of a force sensor. This has been proven to be a well effective method; nevertheless, the focus was on the estimation of task-specific interaction forces, and the extent of the force that the wearer is able to exert on system-controller is not addressed, owing to the fact that the length of the lower limb and the weight of the wearer may differ.

This work is an attempt to modify and generalise the control method in [25] and propose the same for the rehabilitation of individuals with knee or ankle impairment. This study seeks to drive the knee-ankle exoskeleton to follow a predefined rehabilitation trajectory with or without human contribution for a patient in sitting position. To verify the level of contribution of the human the system may allow, a high gain observer is designed. Although high gain observers have been extensively used for the recovery of states such as in [32], in this work the recovered states are employed to verify the level of human contribution. The asymptotic stability of the closed-loop system without human contribution is verified using Lyapunov-based analysis. The convergence of the error between the states of the wearer-exoskeleton and that of the high gain observer is also analysed using Lyapunov stability theory. The contribution of this work is further detailed in Section 5.

2. Mathematical Description of the Knee-Ankle Exoskeleton

This section presents the knee-ankle dynamics and the mathematical model and its state-space form.

2.1. Knee-Ankle Exoskeleton. The knee-ankle exoskeleton is represented by a planar two-link model with revolute joints as shown in Figure 1. The structure and parameters are the same as in [33]. It is made up of two actuators, one at each joint. This model takes into account the flexion/extension of the knee joint and the plantar-flexion/dorsal-flexion of the ankle joint, assuming the motions are performed in a sagittal plane (the basic movement performed by humans such as walking, standing up, sitting down, running, and climbing stairs are examples of sagittal plane movements). This is because exoexercising tasks for lower limbs are those of sagittal plane movements. Sagittal plane model is therefore most often employed in exoskeletal design as in [34, 35] to mention a few.

It should be noted that the parameters of the subject's shank and foot links and that of the exoskeleton are built into the model parameters. The movements of the knee-ankle exoskeleton are in the range $0\,\text{rad} \leq q_1 \leq 2.35\,\text{rad}$

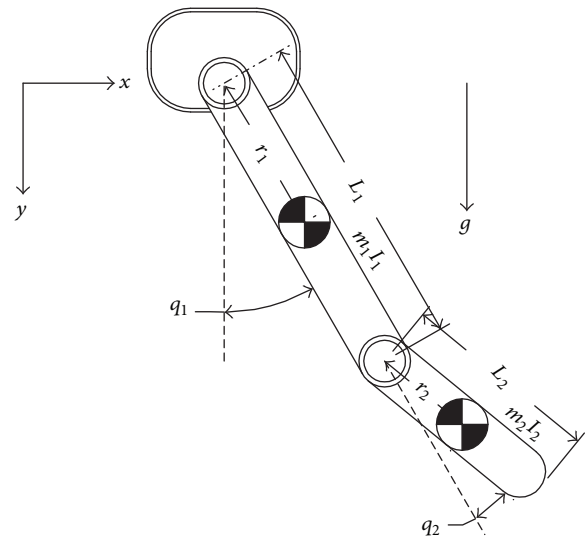

Figure 1: Knee-ankle orthosis.

for the knee and 0 rad $\leq q_2 \leq$ 0.87 rad for the ankle. Where 0 rad relates to the full-knee extension, 2.35 rad is the maximum flexion of the knee, and 1.57 rad corresponds to the rest position of the knee. Furthermore, 0 rad, for the ankle movements, corresponds to the rest position of the ankle, and 0.35 rad is the maximal ankle dorsal-flexion, while 0.87 rad denotes the maximal ankle plantar-flexion. The task will be to devise a control method that will enable the movement of the shank and foot about their respective joints as exoskeleton swings about joint axes concurrently with defined trajectories. This will help provide assistive measures to humans with lower-limb disorders, and consequently requires rehabilitation for improved mobility performance. A sitting position is envisaged for this task; hence the contact forces are not computed and the analysis in [36] concerning floating base systems is not considered. Figure 1 illustrates the model parameters used for this analysis. q_1 is the absolute knee joint angle while q_2 is the relative ankle joint angle (i.e., foot angle).

The need for a reduce number of degrees of freedom (DoF), that is, 2-DoF, for a knee-ankle exoskeleton is to restrict the muscle actuation to the behaviour of each joint required to participate in the actualisation of a certain control task. In addition, numerous DoF may become problematic when included in mathematical models and may eventually cause a drawback in fulfilling the engineering control tasks. Lower numbers of DoF are being assumed for the purpose of simplification [37] so as to reduce its complexity.

The dynamic model of the system may be derived by the Euler-Lagrange principle and written as [38]

$$M(q)\ddot{q} + C(q,\dot{q})\dot{q} + G(q) = \tau. \tag{1}$$

For the purpose of this study, the friction torque, disturbance torque, and the human torque are included; therefore (1) may be modified to give

$$M(q)\ddot{q} + C(q,\dot{q})\dot{q} + G(q) + F(\dot{q}) + \tau_d = \tau + \tau_h, \tag{2}$$

where $q \in \mathfrak{R}^n$ is a vector of angular positions and is assumed available by measurement, $M(q) \in \mathfrak{R}^{n\times n}$ is the inertia matrix of the links, while $\tau \in \mathfrak{R}^n$ is the control torque, which serves as the control inputs of the system, $C(q,\dot{q})\dot{q} \in \mathfrak{R}^n$ is the vector of the Coriolis and centripetal torques, $G(q) \in \mathfrak{R}^n$ is the gravitational torque, and $\tau_h \in \mathfrak{R}^n$ is the human torque, which allows the investigation of the passive and active mode of the wearer. That is, $\tau_h = 0$ implies no human effort and $\tau_h \neq 0$ implies the presence of human effort, and $\tau_d \in \mathfrak{R}^n$ is the disturbance torque, which may be due to measurement noise and is represented as $\tau_d = k_n \text{sgn}(\dot{q})$. k_n is a sine signal and n is the degree of freedom of the system.

The human torque τ_h is stated as

$$\tau_h = \kappa\hat{\tau}, \tag{3}$$

where κ is the variable factor of the level of contribution of the human and $\hat{\tau}$ is the estimated torque.

For simplicity the friction torque $F(\dot{q})$ is written in the form above but may be represented as

$$F(\dot{q}) = F_v\dot{q} + F_d \,\text{sign}(\dot{q}), \tag{4}$$

where $F_v = \text{diag}[v_n]$ is the viscous friction torque and $F_d = \text{diag}[d_n]$ is the dynamic friction torque and v_n and d_n are vector quantities associated with their respective torques. sign$(\cdot)$ is a Signum function.

For clarity purposes, the human and exoskeleton system dynamics may be defined as being summed up in (2). Hence, they may be regarded as $i \in [1, 2]$, which stands for the respective human and exoskeleton components; that is, $M(q) = \sum_{i=1}^{2} M_i(q)$, $C(q,\dot{q}) = C_i(q,\dot{q})$, $G(q) = G_i(q)$, $F_v = F_{v_i}$, and $F_d = F_{d_i}$. In (4), it should be noted that the dynamic friction is balanced so as to make the exoskeleton most transparent to the wearer. The gravity torque is also balanced since the exoskeleton is usually used for rehabilitation purpose.

The matrices associated with $M(q) \in \mathfrak{R}^{n\times n}$, $C(q,\dot{q})\dot{q}$, and $G(q) \in \mathfrak{R}^n$ are given below.

Mass Matrix

$$\begin{aligned} M(q)_{1,1} &= I_1 + I_2 + m_1 L_2^2 + 2m_2 L_1 r_2 \cos(q_2) \\ M(q)_{1,2} &= I_2 + m_2 L_1 r_2 \cos(q_2) \\ M(q)_{2,1} &= I_2 + m_2 L_1 r_2 \cos(q_2) \\ M(q)_{2,2} &= I_2. \end{aligned} \tag{5}$$

Coriolis/Centripetal Vector

$$\begin{aligned} C(q,\dot{q})_{1,1} &= -2m_2 L_1 r_2 \sin(q_2)\dot{q}_2 \\ C(q,\dot{q})_{1,2} &= -m_2 L_1 r_2 \sin(q_2)\dot{q}_2 \\ C(q,\dot{q})_{2,1} &= m_2 L_1 r_2 \sin(q_2)\dot{q}_1 \\ C(q,\dot{q})_{2,2} &= 0. \end{aligned} \tag{6}$$

Gravity Vector

$$\begin{aligned} G(q)_1 &= (m_1 r_1 + m_2 L_1) g \sin(q_1) \\ &\quad + m_2 g r_2 \sin(q_1 + q_2) \\ G(q)_2 &= m_2 g r_2 \sin(q_1 + q_2) \end{aligned} \tag{7}$$

2.2. State-Space Description. To describe the nonlinear state-space form of (2), the human torque τ_h is neglected. This is because it is a fraction of an estimate of the control torque. Since the matrix $M(q)$ is positive definite, it is invertible. Hence, (2) may be written as

$$\ddot{q} = M(q)^{-1}\left(\tau - C(q,\dot{q})\dot{q} - G(q) - F(\dot{q}) - \tau_d\right). \tag{8}$$

The nonlinear state-space form of the dynamic model (1) is given by

$$\dot{x} = f(x) + g(x)\tau, \tag{9}$$

where the state vectors $x : x_1 = \begin{bmatrix} q_1 & q_2 \end{bmatrix}^T$ and $x_2 = \begin{bmatrix} \dot{q}_1 & \dot{q}_2 \end{bmatrix}^T$. The functions $f(x)$ and $g(x)$ are assumed to be continuously differentiable a sufficient number of times.

3. High Gain Observer Structure and Estimation

In wearable robotic systems the coordinates may be precisely measured by an encoder for each joint. However, velocity measurements obtained via tachometers are easily perturbed by noise. These constraints may be overcome by employing an observer for state estimation. The high gain observer is employed for this purpose. Prior to defining the observer dynamics it is necessary to reorganise the state-space model of system in (9) as

$$\begin{aligned} \dot{x}_1 &= x_2 \\ \dot{x}_2 &= f(x) + g(x)\tau = \phi(x_1, x_2, t) \\ y &= x_1, \end{aligned} \tag{10}$$

where y is the measurable position vector.

The state observer is based on the application of high gains, for the system to estimate the angular positions and velocities. The observer in state-space is given by

$$\begin{aligned} \dot{\hat{x}}_1 &= \hat{x}_2 - \frac{1}{\mu} H_p\left(y - \hat{x}_1\right) \\ \dot{\hat{x}}_2 &= \phi(x_1, x_2, t) - \frac{1}{\mu^2} H_v\left(y - \hat{x}_1\right) \end{aligned} \tag{11}$$

with $\hat{x}_1, \hat{x}_2$ denoting the generalised positions and velocities; that is, $\hat{x}_1$ is the estimation of the joint angular position $\begin{bmatrix} q_1 & q_2 \end{bmatrix}$ and $\hat{x}_2$ is the estimation of the joint angular velocities $\begin{bmatrix} \dot{q}_1 & \dot{q}_2 \end{bmatrix}$ and $\hat{x} = [\hat{x}_1^T \quad \hat{x}_2^T]^T$. μ is a scalar parameter chosen with the limit; $0 < \mu < 1$ while H_p and H_v are the two constant observer gains which have the form

$$\begin{aligned} H_p &= \operatorname{diag}\left[h_{pn}\right] \\ H_v &= \operatorname{diag}\left[h_{vn}\right]. \end{aligned} \tag{12}$$

3.1. Observer Error Dynamics. The observer error dynamics between the knee-ankle exoskeleton and the high gain observer may be given by

$$\begin{aligned} \dot{\tilde{x}}_1 &= \hat{x}_2 - \frac{1}{\mu} H_p\left(y - \tilde{x}_1\right) \\ \dot{\tilde{x}}_2 &= \phi(x_1, x_2, t) - \frac{1}{\mu^2} H_v\left(y - \tilde{x}_1\right), \end{aligned} \tag{13}$$

where $\tilde{x}_1 = x_1 - \hat{x}_1$ and $\tilde{x}_2 = x_2 - \hat{x}_2$. $\tilde{x} = [\tilde{x}_1^T \quad \tilde{x}_2^T]^T$ is the error between the system states and the observer states.

For the purpose of the convergence analysis, the error is transformed into a more convenient form as

$$\begin{aligned} \tilde{e}_1 &= \tilde{x}_1 \\ \tilde{e}_2 &= \mu \tilde{x}_2 \\ \tilde{e} &= \begin{bmatrix} \tilde{e}_1^T & \tilde{e}_2^T \end{bmatrix}^T. \end{aligned} \tag{14}$$

Based on the new transformation the error dynamics may be rewritten as

$$\mu \dot{\tilde{e}} = H\tilde{e} + \mu^2 W \phi(x_1, x_2, t), \tag{15}$$

where $H = \begin{bmatrix} -H_p & I_{2\times 2} \\ -H_v & 0_{2\times 2} \end{bmatrix}$ and $W = \begin{bmatrix} 0_{2\times 2} \\ I_{2\times 2} \end{bmatrix}$.

3.2. Convergence Analysis. For clarity, the Lyapunov-based approach in [32] is employed to ascertain the error convergence of the orthosis or exoskeleton states and the high gain observer.

Definition 1. Define the upper bound for the terms $M(q)$, $C(q,\dot{q}), G(q), F_v\dot{q} + F_d \operatorname{sign}(\dot{q})$ and τ_d, in (2), as follows: $\|M(q)\| \le \lambda_0$, $\|C(q,\dot{q})\| \le \lambda_1 \|\dot{q}\|^2$, $\|G(q)\| \le \lambda_2$, $\|F_v\dot{q} + F_d \operatorname{sign}(\dot{q})\| \le \nu\|\dot{q}\| + d_1$, and $\|\tau_d\| \le d_2$. $\|\cdot\|$ is any appropriate norm and λ_i are positive nonzero constants, where $0 < \lambda_i < \infty, \forall i$, and all these properties are applicable $\forall q, e \in \Re^2$ with $\|\tilde{e}\| < \infty$.

With regard to these definitions, the condition for which the nonlinear error dynamics convergence to zero may be found.

Proposition 2. *Consider the dynamic of the system composed of the wearer and the exoskeleton given in (2), with $\tau_h = 0$. With $\tau_h = 0$, no force is being exerted by the user.*

Proof. Consider the quadratic Lyapunov function V for the error dynamics in (15) to be

$$V = \tilde{e}^T P \tilde{e}, \tag{16}$$

where P is the solution to the Lyapunov equation $H^T P + PH = -I$ of a linear system. P is a positive definite matrix and it is independent of μ.

The derivative of V is then given by

$$\dot{V} = \dot{\tilde{e}}^T P \tilde{e} + \tilde{e}^T P \dot{\tilde{e}}. \tag{17}$$

Substituting (15) in (17) gives

$$\begin{aligned} &\left(\frac{1}{\mu} H\tilde{e} + \mu W\phi\right)^T P\tilde{e} + \tilde{e}^T P\left(\frac{1}{\mu} H\tilde{e} + \mu W\phi\right) \\ &= \frac{1}{\mu}\tilde{e}^T \left(H^T P + PH\right)\tilde{e} + 2\mu\phi^T W^T P\tilde{e} \\ &= -\frac{1}{\mu}\|\tilde{e}\|^2 + 2\mu\phi^T W^T P\tilde{e}, \end{aligned} \tag{18}$$

where ϕ is a vector function of the states x_1 and x_2.

Based on (18), the inequality below may be obtained:

$$\dot{V} \leq -\frac{1}{\mu}\|\tilde{e}\|^2 + 2\mu \left\|PW\phi\left(x_1, x_2, t\right)\right\| \|\tilde{e}\|. \tag{19}$$

Define the upper bounded term and a set for the least upper bound as

$$\begin{aligned} \psi(t) &= \left\|PW\phi\left(x_1, x_2, t\right)\right\|, \\ c_T &= \sup_{t\in[0,T]} \psi(t). \end{aligned} \tag{20}$$

Since $\phi(x_1, x_2, t)$ may be defined as the acceleration of the orthotic or exoskeletal device (see (10)), it is therefore upper bounded based on Definition 1 and shows that $\psi(t)$ is upper bounded and c_T exists. P and W are constant matrices.

Assumption 3. Assume that $c_T = \sup_{t\in[0,T]}\psi(t)$ exists for any finite value $T > 0$.

From (19), it follows that

$$\begin{aligned} \dot{V} &\leq -\frac{1}{\mu}\|\tilde{e}\|^2 + \frac{1}{\mu}K_e\left(\mu, c_T\right)\|\tilde{e}\|, \quad \forall t \in [0, T] \\ &= \frac{1}{\mu}\left(K_e\left(\mu, c_T\right) - \|\tilde{e}\|\right)\|\tilde{e}\|, \end{aligned} \tag{21}$$

where $K_e(\mu, c_T) = 2\mu^2 c_T$. K_e is a value determined by μ and c_T. This value remains unchanged when the observer of the orthosis is designed. From (21), it may be deduced that if $\|\tilde{e}\| > K_e(\mu, c_T)$, then $\dot{V} < 0, \forall t \in [0, T]$. Also, based on (20), it may be seen that different cases could arise.

Assumption 4. Assume that $c_T < \infty$.

Then it means that $\|\tilde{e}(t_0)\| \leq K_e(\mu, c_T)$. Therefore, it may be deduced that $\|\tilde{e}\| \leq K_e(\mu, c_T)$, $\forall t \in [0, T]$. The reason is that once $\|\tilde{e}(t_1)\| > K_e(\mu, c_T)$, then the derivative $\dot{V} < 0$, and therefore the norm of the error $\|\tilde{e}\|$ diminishes. By choosing small enough values for μ, the errors between the states of the system and the observer state may be kept small for any finite T.

Assumption 5. Also assume that $\psi(t) \leq \eta$.

And here η represents the bounded range of $[0, \infty)$. Hence, $c = \sup_{t\in[0,\infty)}\psi(t) < \infty$. It may be also seen that if $\|\tilde{e}\| \leq K_e(\mu, c)$, then $\|\tilde{e}(t)\| \leq K_e(\mu, c), \forall t \in \eta$. Also $\|\tilde{e}(t_0)\| > K_e(\mu, c)$ causes the derivative $\dot{V} < 0$ which in turn diminishes $\|\tilde{e}(t)\|$. Therefore, there exists a finite value $t_\mu > 0$ such that $\|\tilde{e}(t)\| \leq K_e(\mu, c) \forall t > t_\mu$.

From the transformed error coordinate in (14), it may be deduced that, for $\mu < 1, \|\tilde{x}\| \leq (1/\mu)\|\tilde{e}\|$. Hence if $\|\tilde{e}\| \leq K_e(\mu, c_T)$, then $\|\tilde{x}\| \leq K_x(\mu, c_T)$, where $K_x(\mu, c_T) = 2\mu c_T$. For any finite value of T, $K_x(\mu, c_T)$ may be made small by making μ small enough. The obtained error convergence proves that the state of the orthosis/exoskeleton may be observed by the high gain observer in (11). Therefore the torque may be estimated based on the recovered states. □

4. Control Law

The formulation of the control law is based on considering the safety of the wearer. It must therefore be sufficiently robust for the stability of the human-orthosis system whether the user is passive or active. The proposed control law is based on [25]. However the generalisation of the control law is considered in this study and it is modified as

$$\begin{aligned} \tau = \mathrm{sat}_{N_1,n}&\left[K_d\dot{\varepsilon} + \mathrm{sat}_{N_2,n}\left(K_p\varepsilon\right)\right] + M\left(q\right)\ddot{q}_d \\ &+ C\left(q, \dot{q}\right)\dot{q}_d + G\left(q\right) + F_v\dot{q} + F_d\,\mathrm{sign}\left(\dot{q}\right), \end{aligned} \tag{22}$$

where $\varepsilon \in \Re^n = q_d - q$ is a vector of the angular position error. $\dot{\varepsilon} \in \Re^n = \dot{q}_d - \dot{q}$ is the vector of the angular velocity error. $\ddot{\varepsilon} \in \Re^n = \ddot{q}_d - \ddot{q}$ is the vector of the angular acceleration error. $q_d \in \Re^n, \dot{q}_d \in \Re^n$, and $\ddot{q}_d \in \Re^n$ signify the desired joint angular position, angular velocity, and angular acceleration, respectively. $K_d = \mathrm{diag}[k_{dn}]$ is the derivative gain while $K_p = \mathrm{diag}[k_{pn}]$ is the proportional gain. $n = 1, 2$.

The definition of the saturation function is given below.

4.1. Saturation Function. The saturation function $\mathrm{sat}_{N_i,n}(x_n)$ is defined as

$$\mathrm{sat}_{N_{i,n}} = \min\left(N_{i,n}, \max\left(-N_{i,n}, x_n\right)\right), \quad \forall x_n \in \Re^n, \tag{23}$$

where $\pm N_{i,n}$ represent the saturation bounds. This bounded interval (point) is chosen such that $N_{1,n} > 2N_{2,n}$. The saturation of the control law allows the actuator of the

exoskeleton to avoid exceeding its limit, thereby maintaining the linearity of the actuator and avoiding the hysteresis cycles which may result in irreversible damage. This guarantees the stability of the closed-loop trajectories. High value control law demands high power and may expose the user to risk.

4.2. Closed-Loop System. The dynamics of the closed-loop system are achieved by substituting (4) into (2) and then substituting the eventual equation into (22). The resulting equation is given by

$$M(q)\ddot{\varepsilon} = -\text{sat}_{N_1,n}\left[K_d\dot{\varepsilon} + \text{sat}_{N_2,n}\left(K_p\varepsilon\right)\right] - C(q,\dot{q})\dot{\varepsilon} - \tau_h. \tag{24}$$

Note that τ_d for the purpose of the proof is not included in the closed-loop system equation.

4.3. Stability Analysis. Here, the closed-loop stability of the entire system (orthotic/exoskeletal device and controller) is verified. A completely passive mode (i.e., $\tau_h = 0$) for the user is considered. Passive mode refers to a user exerting no muscular torque that may interfere with the orthosis/exoskeleton trajectory, as specified by the physiotherapist. The stability for the system's equilibrium point is proven. For the purpose of this proof consider $N_{i,n} \in \mathfrak{R}^n$.

Proposition 6. *Consider the wearer-exoskeleton dynamics defined by (2), with $\tau_h = 0$. With $\tau_h = 0$, no force is being exerted by the user.*

Assumption 7. Assume that the derivatives of the desired angle ($\dot{q}_d, \ddot{q}_d$ and $q_d^{(3)}$) are bounded and known.

Then the equilibrium point $x_e = [\varepsilon^T \quad \dot{\varepsilon}^T]^T = 0 \in \mathfrak{R}^{2n}$ of the closed-loop system (24) is asymptotically stable.

Proof. Let $K_p|\varepsilon| > N_{2,n}$ and $K_d|\dot{\varepsilon}| > N_{1,n} - N_{2,n} > N_{2,n}$, defining the positive definite Lyapunov function V_1 to be

$$V_1 = \frac{1}{2}\dot{\varepsilon}^T M(q)\dot{\varepsilon}. \tag{25}$$

The derivative of $\dot{V}_1$ is given by

$$\dot{V}_1 = \dot{\varepsilon}^T M(q)\ddot{\varepsilon} + \frac{1}{2}\dot{\varepsilon}^T\dot{M}(q)\dot{\varepsilon}. \tag{26}$$

Substituting (24) into (26) gives $\dot{V}_1$ as

$$\dot{V}_1 = -\dot{\varepsilon}^T\left(\text{sat}_{N_1,n}\left[K_d\dot{\varepsilon} + \text{sat}_{N_2,n}\left(K_p\varepsilon\right)\right] - C(q,\dot{q})\dot{\varepsilon} - \tau_h\right) + \frac{1}{2}\dot{\varepsilon}^T\dot{M}(q)\dot{\varepsilon}. \tag{27}$$

If $\tau_h = 0$, the derivative V_1 is

$$\dot{V}_1 = -\dot{\varepsilon}^T\text{sat}_{N_1,n}\left[K_d\dot{\varepsilon} + \text{sat}_{N_2,n}\left(K_p\varepsilon\right)\right] - \dot{\varepsilon}^T C(q,\dot{q})\dot{\varepsilon} + \frac{1}{2}\dot{\varepsilon}^T\dot{M}(q)\dot{\varepsilon}. \tag{28}$$

By factorisation, (28) may be rewritten as

$$\dot{V}_1 = -\dot{\varepsilon}^T\text{sat}_{N_1,n}\left[K_d\dot{\varepsilon} + \text{sat}_{N_2,n}\left(K_p\varepsilon\right)\right] + \frac{1}{2}\dot{\varepsilon}^T\left(\dot{M}(q) - 2C(q,\dot{q})\right)\dot{\varepsilon}. \tag{29}$$

The matrices $\dot{M}(q)$ and $C(q,\dot{q})$ are dependant, as the following relation is satisfied by the second term in (29); therefore, $\dot{\varepsilon}^T S\dot{\varepsilon} = (1/2)\dot{\varepsilon}^T(\dot{M}(q) - 2C(q,\dot{q}))\dot{\varepsilon} = 0$, where S is skew symmetric. Then (29) becomes

$$\dot{V}_1 = -\dot{\varepsilon}^T\text{sat}_{N_1,n}\left[K_d\dot{\varepsilon} + \text{sat}_{N_2,n}\left(K_p\varepsilon\right)\right]. \tag{30}$$

If $|K_d\dot{\varepsilon}| > N_{2,n}$, by observation $\dot{\varepsilon}$ and $K_d\dot{\varepsilon} + \text{sat}_{N_2,n}(K_p\varepsilon)$ have the same sign and certainly $|K_d\dot{\varepsilon} + \text{sat}_{N_2,n}(K_p\varepsilon)| > 0$. With regard to this, $\dot{V}_1$ may be reduced to

$$\dot{V}_1 = -\lambda\left|\dot{\varepsilon}^T\right|N_{1,n} \le 0. \tag{31}$$

It may therefore be assumed that as $|\dot{\varepsilon}^T|$ decreases $\dot{V}_1$ decreases also. Note that λ is any positive value to derive the inequality for checking the negativeness of $\dot{V}_1$. However, based on this, no conclusion may be reached with regard to its asymptotic stability. To establish this, a second Lyapunov function is chosen considering a velocity reference signal and the filtered tracking error.

Definition 8. Define the velocity reference signal as $\dot{q}_r = \dot{q}_d - \Gamma\varepsilon$ and the filtered error as $s = \dot{q}_r - \dot{q} = \dot{\varepsilon} - \Gamma\varepsilon$, $\Gamma = \text{diag}[\gamma_i] > 0$. Hence, $\dot{s} = \ddot{q}_r - \ddot{q} = \ddot{\varepsilon} - \Gamma\dot{\varepsilon}$.

Based on Definition 8, the following equation holds:

$$M(q)[\dot{s} + k_1 s] + C(q,\dot{q})s = M(q)[\ddot{q}_r - k_1 s] + C(q,\dot{q})\dot{q}_r - [M(q)\ddot{q} + C(q,\dot{q})\dot{q}], \tag{32}$$

where $M(q)k_1 \ge 0$ and commutative. $k_1 = \text{diag}[\alpha] \ge 0$. Substituting (2) into (32) yields

$$M(q)[\dot{s} + k_1 s] + C(q,\dot{q})s = M(q)[\ddot{q}_r - k_1 s] + C(q,\dot{q})\dot{q}_r - [\tau + \tau_h - G(q) - F_v\dot{q} - F_d\,\text{sign}(\dot{q})]. \tag{33}$$

Assumption 9. From (22), consider an equivalence controller of the form

$$\tau = \text{sat}_{N_1,n}\left[K_d\dot{s} + \text{sat}_{N_2,n}\left(K_p s\right)\right] + M(q)[\ddot{q}_r - k_2 s] + C(q,\dot{q})\dot{q}_r + G(q) + F_v\dot{q} + F_d\,\text{sign}(\dot{q}), \tag{34}$$

where k_2 is of the same form as k_1.

Introducing (34) into (33) results in the closed-loop system with regard to (2).

$$M(q)\dot{s} = -Ks - \text{sat}_{N_1,n}\left[K_d\dot{s} + \text{sat}_{N_2,n}\left(K_p s\right)\right] - C(q,\dot{q})s, \tag{35}$$

where $K = M(q)(2k_1 - k_2)$.

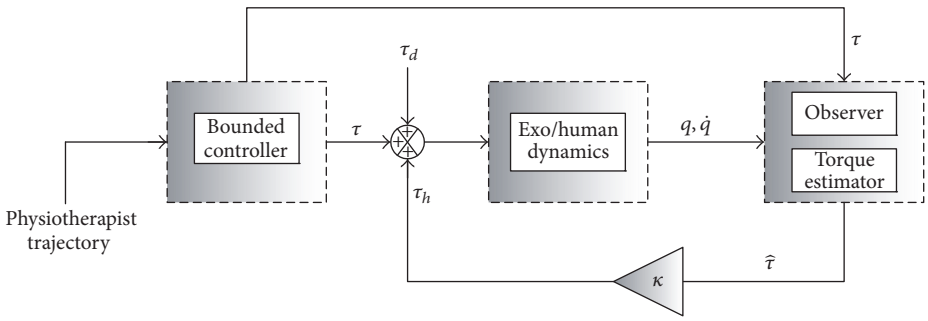

Figure 2: Block diagram of the observer-based controller.

Consider the Lyapunov function

$$V_2 = \frac{1}{2} s^T M(q)\, s. \tag{36}$$

The derivative of V_2 may be given as

$$\dot{V}_2 = s^T M(q)\, \dot{s} + \frac{1}{2} s^T \dot{M}(q)\, s. \tag{37}$$

Substituting (35) into (37) gives

$$\begin{aligned} \dot{V}_2 = {} & -s^T K s - s^T \mathrm{sat}_{N_1,n}\left[K_d \dot{s} + \mathrm{sat}_{N_2,n}\left(K_p s\right)\right] \\ & + \frac{1}{2} s^T \left(\dot{M}(q) - 2C(q,\dot{q})\right) s. \end{aligned} \tag{38}$$

$(1/2)s^T(\dot{M}(q) - 2C(q,\dot{q}))s = 0$ based on the skew symmetric properties as previously stated. The derivative of V_2 therefore becomes

$$\dot{V}_2 = -s^T K s - s^T \mathrm{sat}_{N_1,n}\left[K_d \dot{s} + \mathrm{sat}_{N_2,n}\left(K_p s\right)\right]. \tag{39}$$

Using the same principle as in (30), $\dot{V}_2$ can be reduced to

$$\dot{V}_2 = -s^T K s - \lambda \left|s^T\right| N_1, \quad n \le 0, \tag{40}$$

where λ is the same as previously defined.

This then leads to $-\dot{V}_2(0) \le \dot{V}_2(t)$. Consequently, the boundedness of $\dot{s}$, s, and $\dot{\varepsilon}$ subsequently leads to $e \to 0$ as $t \to \infty$. Based on the above choice of different Lyapunov function (V_1 and V_2), the need for the Mastrov theorem for conclusion of asymptotic stability is eliminated. □

5. Problem Formulation

The objective of this paper is to formulate a strategy by which the human force (torque) sensitivity during the design and operation phases of an orthosis can be evaluated. This is to be achieved by the following:

(1) First is setting actuator size limit for the exoskeleton by means of nested saturation.

(2) Second is reconstruction of the control torque via the recovered states using the observer. A portion is then fed back to act as the human torque, mimicking the exertion of the force of the human-in-the-loop.

(3) Verification of this principle is based on the utilisation of a robust bounded control strategy with balanced gravity torque and friction to make the orthosis as transparent as possible to the wearer.

(4) Convergence analysis and asymptotic stability are therefore proven to mathematically validate the proposed principle.

The orthosis control with human-in-the-loop requires three building blocks; the dynamics of the wearer-exoskeleton, the controller, and the observer/torque estimator (see Figure 2.) Here, the mathematical equation for the torque estimator and the reference inputs are presented.

The physiotherapist trajectories for the knee and ankle are chosen to fit within the limits of their range of motions and are given by

$$\begin{aligned} q_1 &= \frac{3\pi}{2} \sin\left(\frac{2\pi}{3} t\right) \\ q_2 &= \frac{\pi}{6} \sin\left(\frac{\pi}{2} t\right). \end{aligned} \tag{41}$$

Furthermore, the high gain observer used for the estimation of the angular positions and velocities is analysed in Section 3. The estimation of the torque is derived from these values based on the equation

$$\widehat{\tau} = M\left(\widehat{q}\right)\ddot{\widehat{q}} + C\left(\widehat{q},\dot{\widehat{q}}\right)\dot{\widehat{q}} + G\left(\widehat{q}\right) + F_v\dot{\widehat{q}} + F_d \,\mathrm{sign}\left(\dot{\widehat{q}}\right), \tag{42}$$

where all the parameters in the equation are same as that in (2) but represent the estimated version.

6. Simulations Results and Discussion

For the purpose of clarity, three cases have been considered. For each case, the simulations were channeled towards the validation of the control strategy hence showing its robustness. In addition the following variables used in the simulation results are described below:

(i) q_1 is the knee joint angle (position).

(ii) q_2 is the ankle joint angle (position).

(iii) $\dot{q}_1$ is the derivative (velocity) of knee joint angle.

Table 1: Physiological parameters *(Case 1 & Case 2)*.

Parameters	Units	Values
Shank length (L_1)	m	0.2000
Foot length (L_2)	m	0.0800
Shank mass (m_1)	kg	2.8000
Foot mass (m_2)	kg	1.1700
Shank inertia (I_1)	kg·m^2	0.0750
Foot inertia (I_2)	kg·m^2	0.0120
gravity (g)	m/s^2	9.8000
Shank damping Coeff. (b_1)	Nm/s^2	0.4000
Foot damping Coeff. (b_2)	Nm/s^2	0.6000
Knee joint angle ($q_1(0)$)	rad	0.5000
Ankle joint angle ($q_2(0)$)	rad	0.2000
Knee joint friction (v_1)	rad	2.3500
Ankle joint friction (v_2)	rad	0.8700
$k_n(\tau_d)$	rad	$5\sin(4\pi t)$

(iv) $\dot{q}_2$ is the derivative (velocity) of ankle joint angle.

(v) q_{d1} is the desired knee joint angle (position).

(vi) q_{d2} is the desired ankle joint angle (position).

(vii) $\dot{q}_{d1}$ is the derivative (velocity) of desired knee joint angle.

(viii) $\dot{q}_{d2}$ is the derivative (velocity) of desired ankle joint angle.

(ix) $\widehat{q}_1$ is the estimated knee joint angle (position).

(x) $\widehat{q}_2$ is the estimated ankle joint angle (position).

(xi) $\dot{\widehat{q}}_1$ is the derivative (velocity) of the estimated knee joint angle.

(xii) $\dot{\widehat{q}}_2$ is the derivative (velocity) of the estimated ankle joint angle.

6.1. Case 1. In this case, the physiological parameters used are those of Table 1, with the exception of the d_n and v_n. Hence, arbitrary values of $d_n = 2.35$ rad and $v_n = 0.87$ rad were chosen for the purpose of simulation. For this bounded control law, it is desired that the maximal motor torque is 15 Nm for both joint torques. The saturation bounds $N_{1,1}$ and $N_{1,2}$ are chosen to be 7.6 Nm for both joints, whereas $N_{2,1}$ and $N_{2,2}$ are chosen to be 7.6/2.1 Nm for both joints as well. The controller gains for K_p are 15.2180×10^2 and 9.4500×10^2 for the knee and ankle joints and K_d are 0.2840×10^3 and 0.6720×10^3 for the respective joints. The observer gains $h_{v1} = 15.5$, $h_{v2} = 14.2$, $h_{p1} = 10.5$, and $h_{p2} = 12.5$, while μ is set to 0.01. The gains of the system-controller are manually tuned to find the best fit. This is the same for the observer gain. Due to the presence of control chattering activity induced by the saturation function, the control gains required to ensure a good tracking performance somehow increase. This justifies the high gains needed for this controller.

In *Case 1*, three scenarios were studied, where the desired trajectory is expected to be tracked by the wearer in each scenario despite the condition introduced. These scenarios are discussed below.

6.1.1. Scenario 1. In the first scenario, the wearer is completely passive (complete motor function disorder); that is, $\tau_h = 0$ (see Figures 3, 4, and 5). The controller is seen to perform the task of making the user completely track the desired angular position and velocity trajectories, at a considerable time. The torque input is within the limits of 15 Nm and hence the saturation of the actuators is avoided. The observer's ability to correctly estimate the position and velocity trajectories is also guaranteed.

6.1.2. Scenario 2. In the second scenario, two simulations that show the wearer, providing a percentage of the human torque used in resisting the orthosis control ability to track the desired angular position and velocity trajectories are presented (see Figures 6, 7, 8 and 9) for the first simulation and (see Figures 10, 11, 12, and 13) for the second simulation. In both cases, the human torque $\tau_h \neq 0$, and it is a percentage of the estimated torque given by $\tau_h = \kappa\widehat{\tau}$, where $\kappa = 0.1$ and 0.2. The angular position and velocity trajectory tracking are also accomplished and the control torque inputs have a higher value. The higher the resistive torque, the higher the control torque value. This is because the controller has to produce greater torque to overcome the resistance of the wearer. The resistive human torque is achieved by inverting a fraction of the estimated torque. This may be seen in Figures 9 and 13. However, since it is within a specified limit, the torque input should not be allowed to overcome the specified limit to avoid saturation. Although the maximal torque is somewhat exceeded by a small percentage, a considerable tolerance actuator value in the physical system could compensate for this. Beyond these limits, saturation occurs. The main interest is to ensure that the wearer safety is still guaranteed; hence setting the torque limit to 15 Nm satisfies this condition.

6.1.3. Scenario 3. In the third scenario, an assistive human torque provided by the wearer to assist the orthosis control in order to track the desired angular position and velocity trajectories is verified (see Figures 14, 15, 16, and 17). The assistive human torque ($\tau_h \neq 0$) provided is 10% of the estimated torque. The angular position and velocity trajectory tracking are guaranteed as required, but the control torque inputs have a smaller value. This is due to the assistance provided by the wearer. The assistive human torque is achieved by inputting a fraction of the estimated torque directly in contrast to the resistive torque applied. This may be seen in Figure 17. It should be noted that the second and the third scenarios exemplify a partial motor function disorder.

6.2. Case 2. The value of the torque input of the system may depend on its parameters and the external loads. However, applying high value control law may lead to a high power requirement to ensure it. Wearable orthosis/exoskeleton is characteristically equipped with on-board power system and

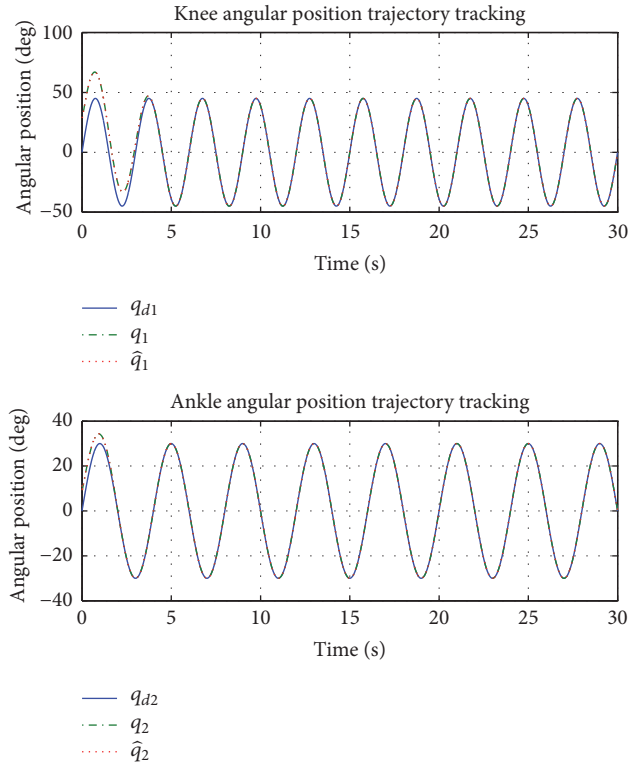

FIGURE 3: Knee-ankle position trajectory tracking. $\tau_h = 0$ *(Scenario 1 of Case 1).*

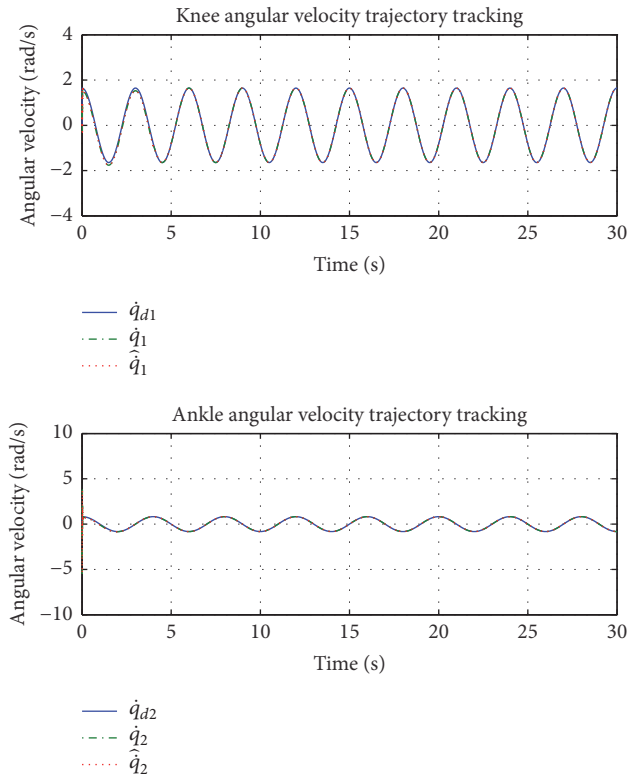

FIGURE 4: Knee-ankle velocity trajectory tracking. $\tau_h = 0$ *(Scenario 1 of Case 1).*

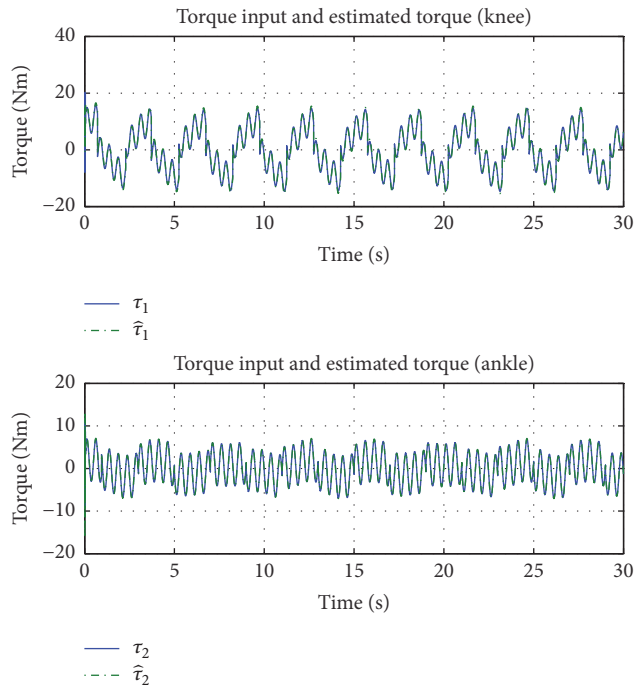

FIGURE 5: Knee-ankle torque input and estimated torque. $\tau_h = 0$. This is to exemplify a complete motor function disorder when the wearer is completely passive. The estimated torque is plotted to show that the observer can correctly estimate the exoskeleton state; hence the torque can be reconstructed *(Scenario 1 of Case 1)*.

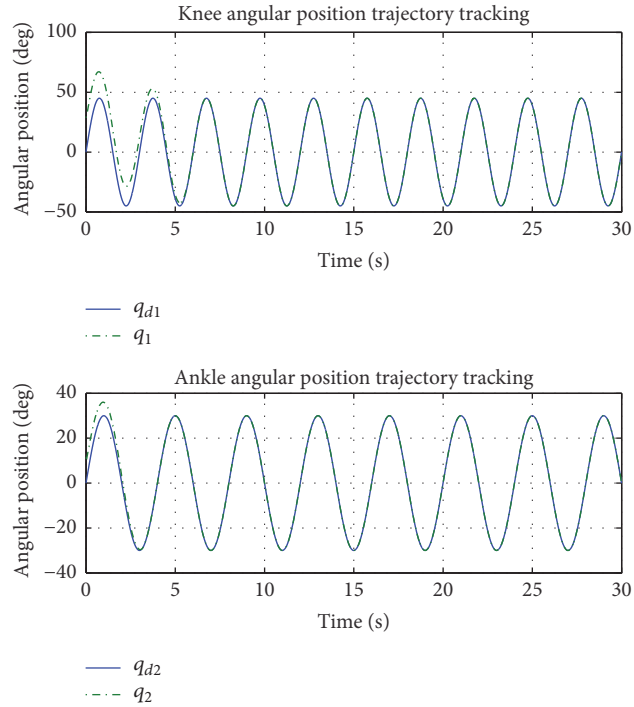

FIGURE 6: Knee-ankle position trajectory tracking. $\tau_h \neq 0$; $\kappa = 0.1$ *(Scenario 2 of Case 1)*.

hence needs high power demands that may endanger the wearer. To reduce this high value control law effect the nested saturation (bounded control) is employed so that the actual actuator size limit can be set. This has been established in *Scenario 2 and 3 of Case 1*.

For the purpose of clarity, an actuator size of 30 Nm is considered. Using the same physiological parameters as in Table 1, controller gains and other parameters with the exception of the saturation bounds which are chosen as 15.1 Nm for $N_{1,1}$ and $N_{1,2}$ for both joints and

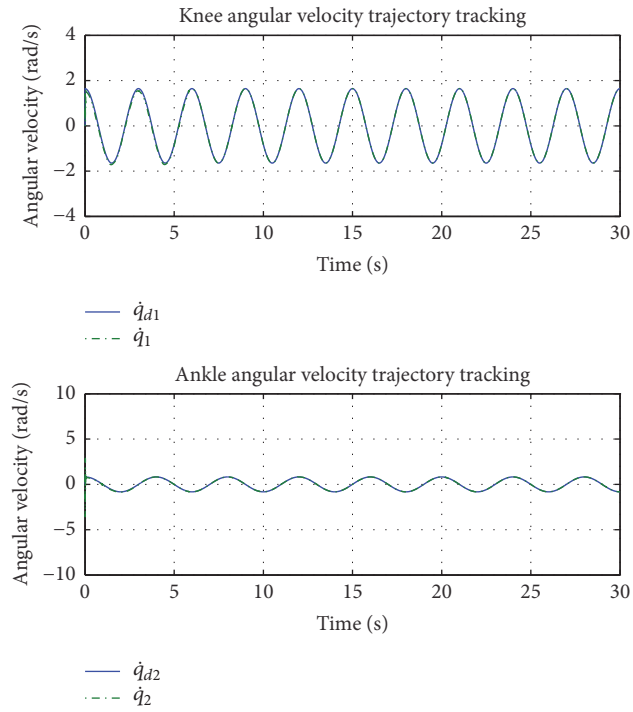

FIGURE 7: Knee-ankle velocity trajectory tracking. $\tau_h \neq 0$; $\kappa = 0.1$ *(Scenario 2 of Case 1)*.

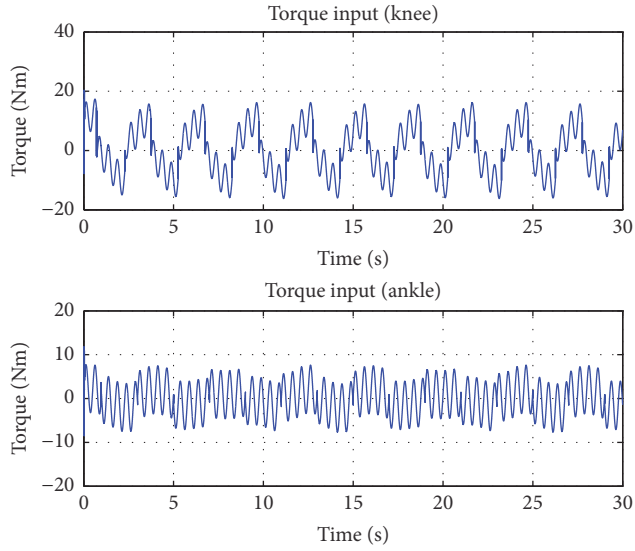

FIGURE 8: Knee-ankle torque input. $\tau_h \neq 0$; $\kappa = 0.1$. Considering the human resistive torque in Figure 9, that is, the human is exerting a force capable of resisting the orthosis control ability to track the physiotherapist trajectory, hence there is an increase in the control torque required to perform the task *(Scenario 2 of Case 1)*.

also 15.1/2.1 Nm for $N_{2,1}$ and $N_{2,2}$ for both joints as well.

In this test case, a resistive human torque is applied as in *Scenario 2 of Case 1*. With the same task needed to be performed, an inverted fraction of the control torque, which is based on the state observer is fed back to the system as the human torque. Given the actuator limit as 30 Nm, the system allows a maximum of $\kappa = 0.5$ of the resistive human torque ($\tau_h \neq 0$) to be applied corresponding to 50% of the estimated torque. Beyond this limit the actuator is saturated. Figure 20 shows the control torque input required for the physiotherapist task to be performed based on the resistive human torque applied to the system. The resistive human torque applied is shown in Figure 21. Figures 18 and

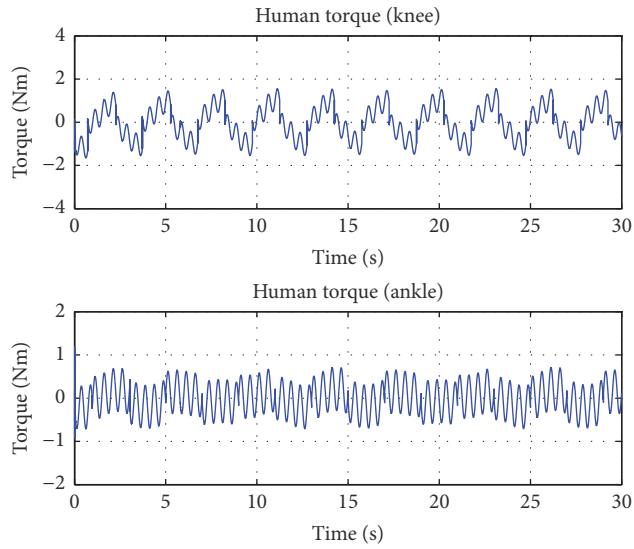

FIGURE 9: Knee-ankle human torque input (resistive torque). $\tau_h \neq 0$; $\kappa = 0.1$. The amount of human torque exerted on the orthosis is shown in this figure, which is 10% of the estimated torque *(Scenario 2 of Case 1)*.

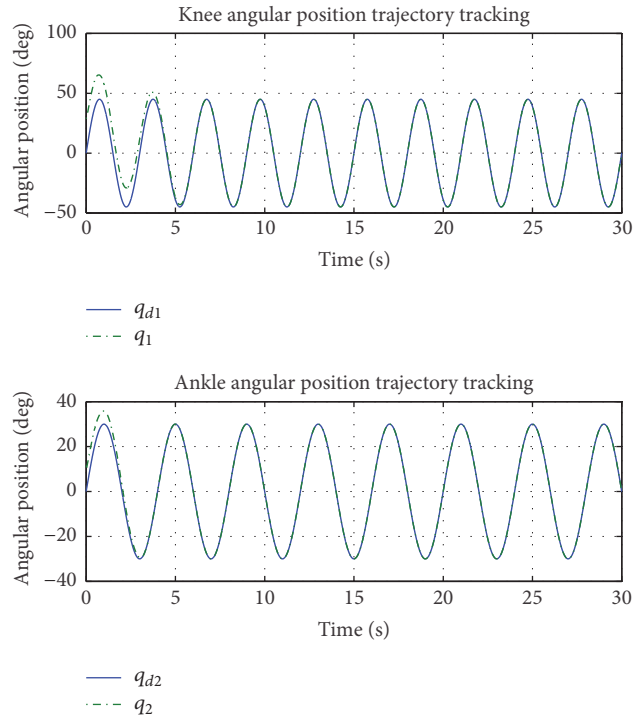

FIGURE 10: Knee-ankle position trajectory tracking. $\tau_h \neq 0$; $\kappa = 0.2$ *(Scenario 2 of Case 1)*.

19 present the position and velocity trajectory tracking of the controller. This is a proof of the controller's ability to ensure the task is performed even in the presence of the resistive human force. However, the effect of the disturbance is seen in the estimated state. In addition, considering Figure 12 in comparison with Figure 20, it may be deduced that, for a system of this nature with same system parameters, the higher the actuator limit the higher the amount of resistive human torque it may allow (axis of Figure 20 is slightly increased to accommodate the increase in torque input).

6.3. Case 3. For the purpose of robustness, the bounded controller is tested using the system parameters for a lower-limb orthosis described in [39, 40]. These system parameters are given in Table 2, the values of which are calculated using 1.5 m of the human limb length and a weight of 65 kg. The

Table 2: Physiological parameters *(Case 3)*.

Parameters	Units	Values
Shank length (L_1)	m	0.3690
Foot length (L_2)	m	0.2280
Shank mass (m_1)	kg	2.9900
Foot mass (m_2)	kg	0.9425
Shank inertia (I_1)	kg·m^2	0.0339
Foot inertia (I_2)	kg·m^2	0.0041

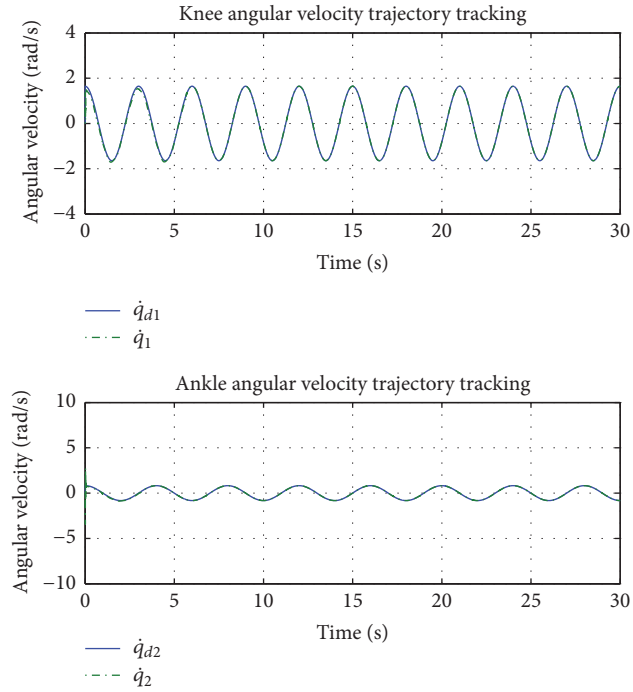

Figure 11: Knee-ankle velocity trajectory tracking. $\tau_h \neq 0$; $\kappa = 0.2$ *(Scenario 2 of Case 1)*.

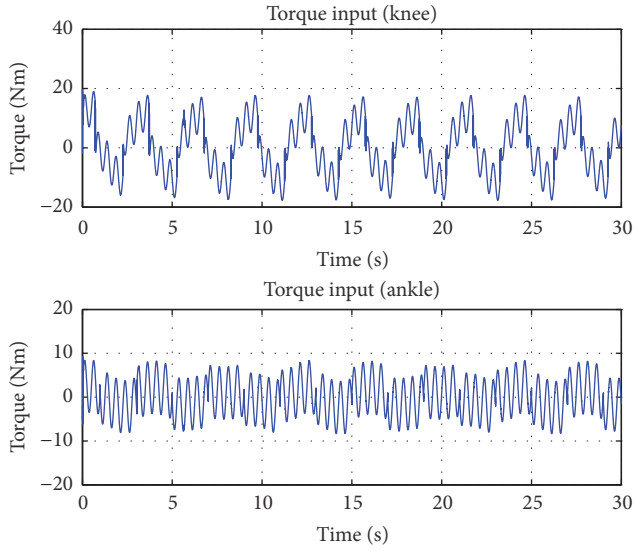

Figure 12: Knee-ankle torque input. $\tau_h \neq 0$; $\kappa = 0.2$. Considering the human resistive torque in Figure 13, that is, the human is exerting a force capable of resisting the orthosis control ability to track the physiotherapist trajectory, hence there is a further increase in the control torque required to perform the task as compared to Figure 8 *(Scenario 2 of Case 1)*.

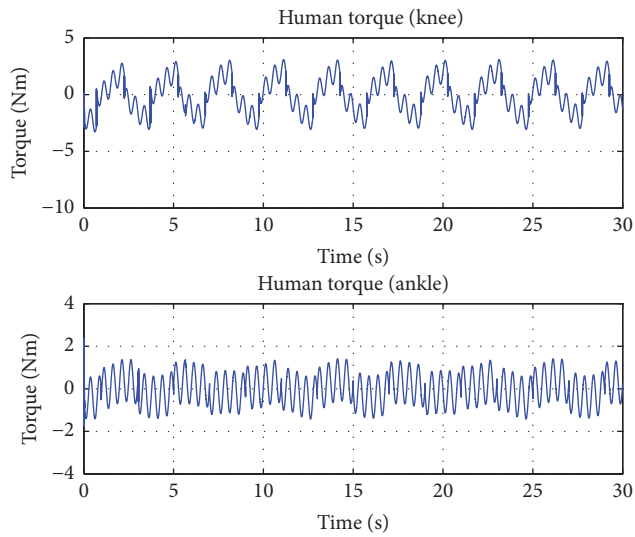

FIGURE 13: Knee-ankle human torque input (resistive torque). $\tau_h \neq 0; \kappa = 0.2$. The amount of human torque exerted on the orthosis is shown in this figure, which is 20% of the estimated torque. However, the torque signal is inverted for this purpose *(Scenario 2 of Case 1)*.

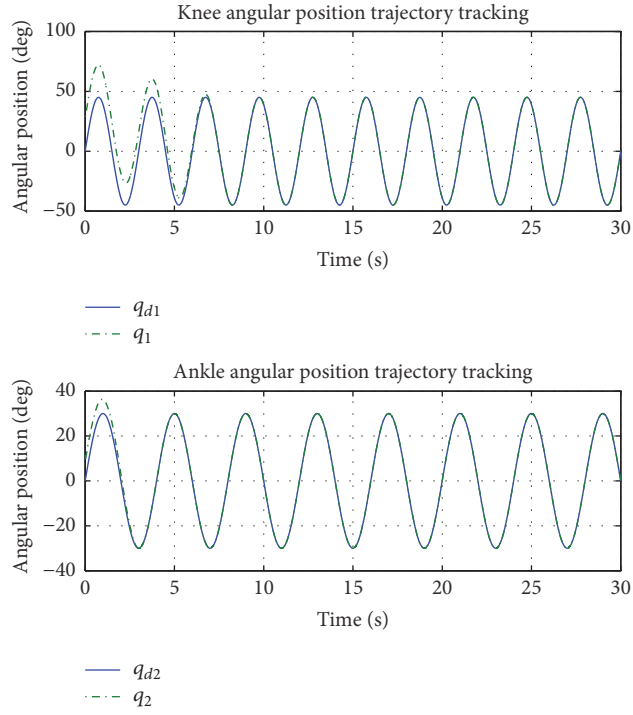

FIGURE 14: Knee-ankle position trajectory tracking. $\tau_h \neq 0; \kappa = 0.1$ *(Scenario 3 of Case 1)*.

moments of inertia are computed using $mL^2/12$, assuming the center of mass to be at the center of each cylindrical link (see Figure 1). Other parameters not given in Table 2 are the same as in Table 1.

In this test case, the saturation bounds are the same as in *Case 1*, and hence the maximum actuator size considered is 15 Nm. The controller gains for K_p are tuned to be 9.5435×10^2 and 4.0706×10^2 for the knee and ankle joints and for K_d are 0.3044×10^3 and 0.4716×10^2 for the respective joints. The observer gains are the same as in *Case 1*.

From Figure 24, it may be seen that the torque inputs are within the actuator size limit, and the estimated torques are correctly estimated with regard to the recovered (observer) state. Figures 22 and 23 show that the controller has the ability to ensure the wearer-exoskeleton is able to track the position and velocity of the physiotherapist trajectory in

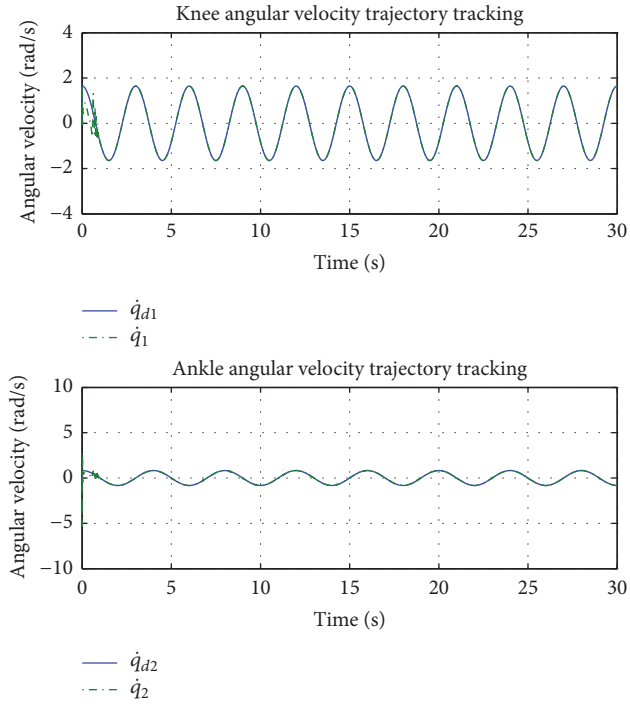

FIGURE 15: Knee-ankle velocity trajectory tracking. $\tau_h \neq 0$; $\kappa = 0.1$ *(Scenario 3 of Case 1)*.

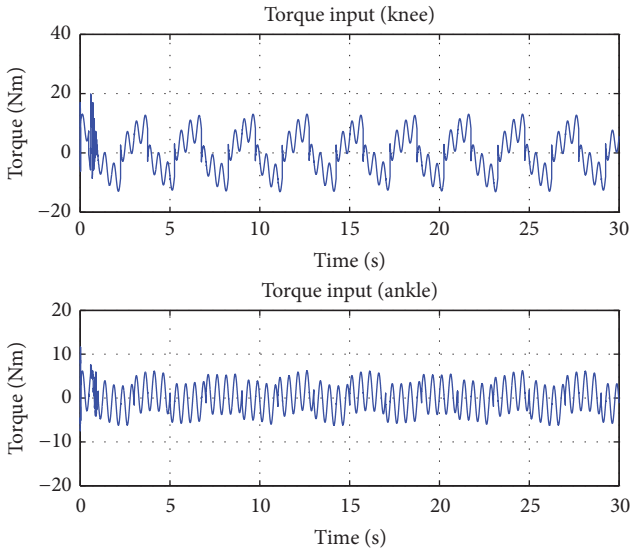

FIGURE 16: Knee-ankle torque input. $\tau_h \neq 0$; $\kappa = 0.1$. Considering the human assistive torque in Figure 17, that is, the human is exerting a force capable of assisting the orthosis control ability to track the physiotherapist trajectory, hence there is a decrease in the control torque required to perform the task *(Scenario 3 of Case 1)*.

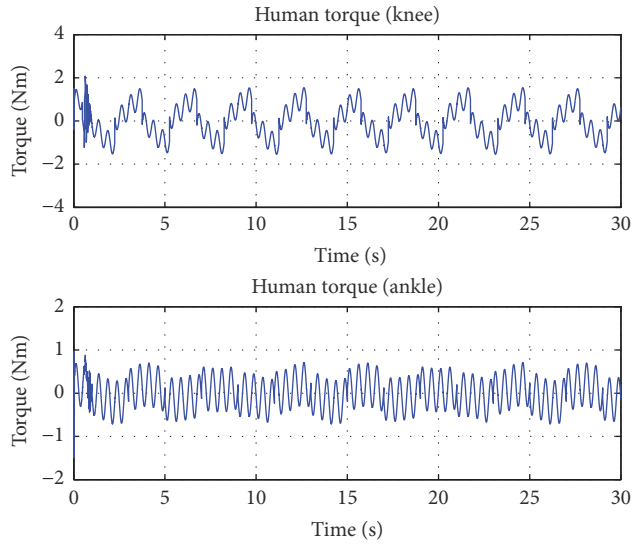

FIGURE 17: Knee-ankle human torque input (assistive torque). $\tau_h \neq 0$; $\kappa = 0.1$. The amount of human torque exerted on the orthosis is shown in this figure, which is 10% of the estimated torque *(Scenario 3 of Case 1)*.

spite of the variation in system parameters. The controller robustness is therefore established. Note that the wearer is completely passive in this case and the limit is same as in *case 1*.

7. Conclusion and Future Work

Developing an exoskeleton device needs a well-designed control system so as to ensure the wearer is not further injured by the device. It is therefore necessary that the controller is robust enough to actualise its capability. In this study,

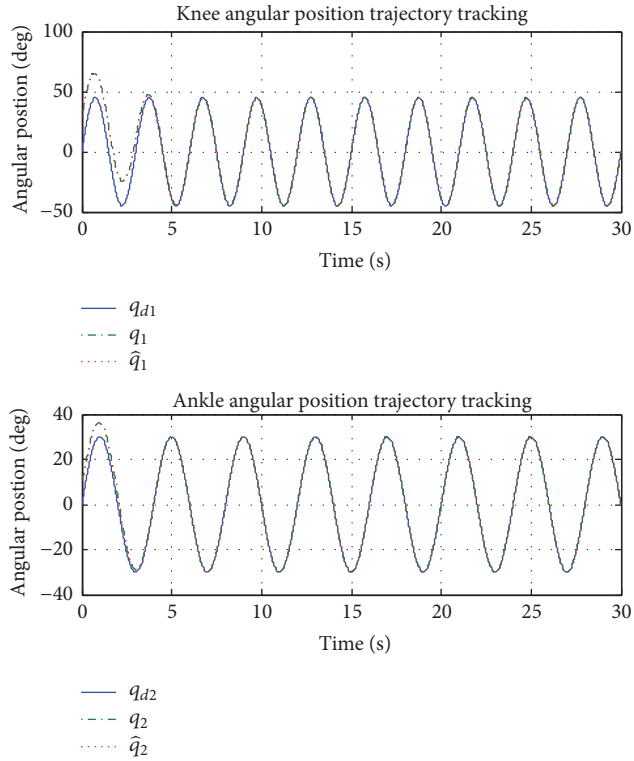

FIGURE 18: Knee-ankle position trajectory tracking. $\tau_h \neq 0; \kappa = 0.5$ *(Case 2)*.

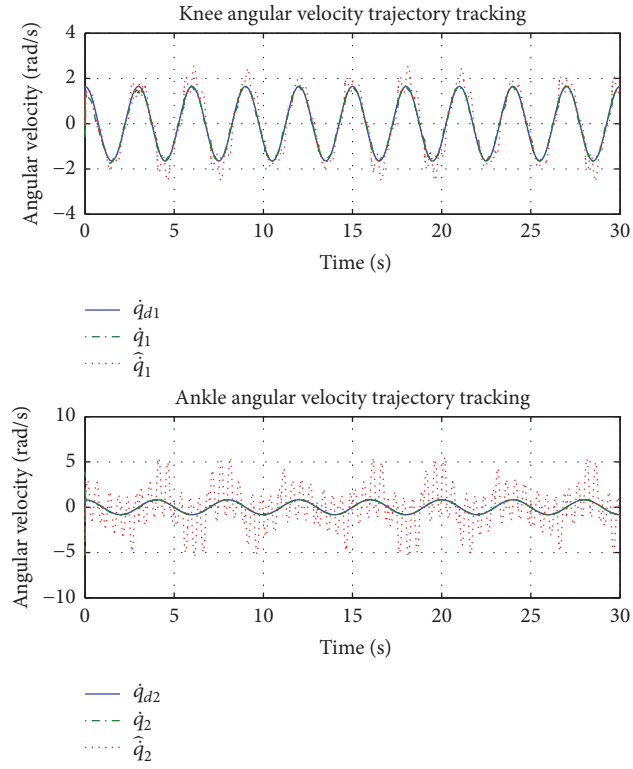

FIGURE 19: Knee-ankle velocity trajectory tracking. $\tau_h \neq 0; \kappa = 0.5$ *(Case 2)*.

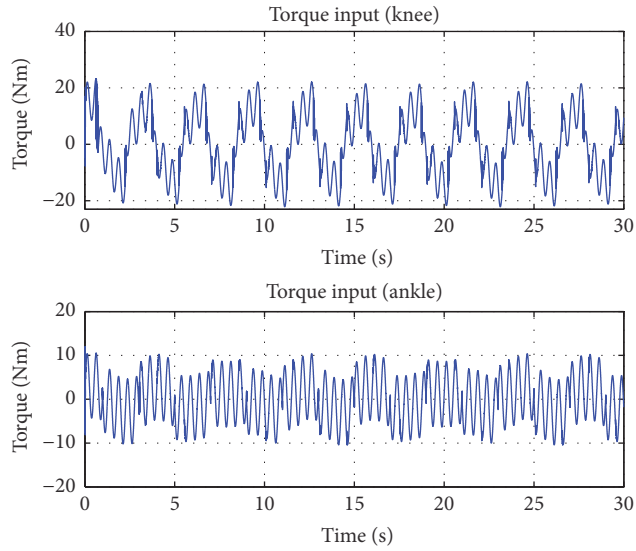

FIGURE 20: Knee-ankle torque input. $\tau_h \neq 0; \kappa = 0.5$. Considering the human resistive torque in Figure 17, that is, the human is exerting a force capable of assisting the orthosis control ability to track the physiotherapist trajectory, hence there is an increase in the control torque required to perform the task *(Case 2)*.

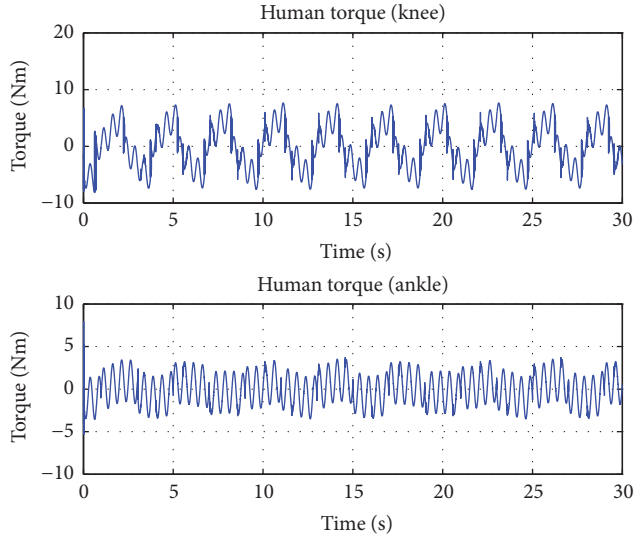

FIGURE 21: Knee-ankle human torque input (resistive torque). $\tau_h \neq 0; \kappa = 0.5$. The amount of human torque exerted on the orthosis is shown in this figure, which is 50% of the estimated torque *(Case 2)*.

a bounded nonlinear feedback controller in conjunction with a high gain observer is proposed for the rehabilitation of the user and the determination of the level of contribution a wearer can offer for a specific exoskeleton. The level of contribution helps demonstrate the partial motor function disorder; that is, the user may be able to exact a certain amount of human torque. This was tested via MATLAB/SIMULINK simulations for a knee-ankle orthosis model. Simulation results obtained help to establish this fact. This is established by using three test cases to analyse the exact purpose of this work. In addition to the controller robustness, its ability to avoid the saturation of the actuators has been verified. It is to be noted that the wearer is in a sitting position. Lyapunov-based analysis to prove the asymptotic stability of the controller and the convergence of the observer has also been presented.

In future works, the controller is expected to be tested in the laboratory. It is expected that parametric identification is first carried out before it is tested in real time. The input-to-state stability (ISS) will also be verified. Other future areas of research interest include robot axes misalignments, which constitute a major difficulty in the design of exoskeleton.

Conflicts of Interest

The authors declare that they have no conflicts of interest.

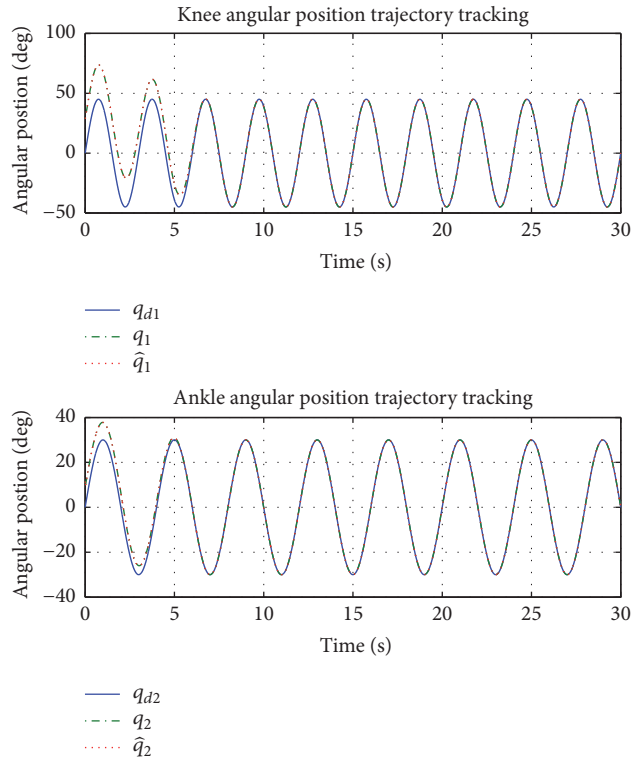

FIGURE 22: Knee-ankle position trajectory tracking. $\tau_h = 0$ *(Case 3)*.

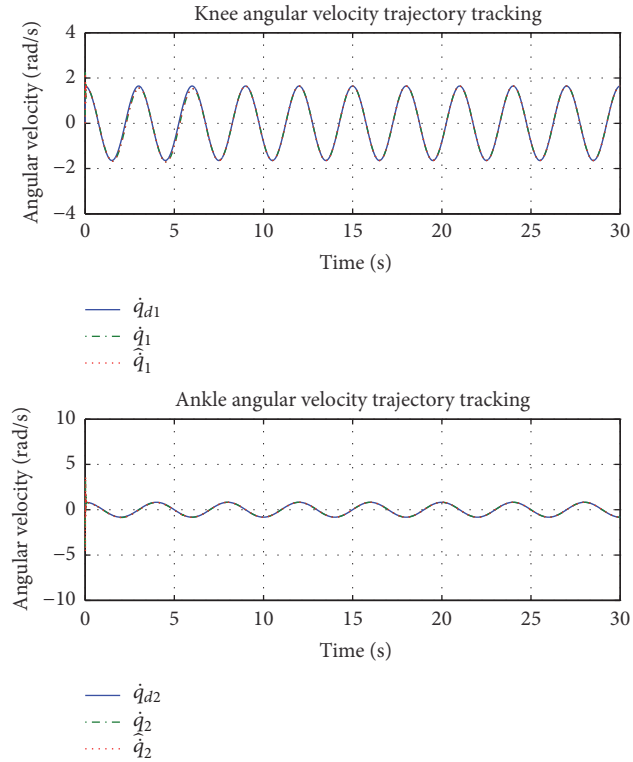

FIGURE 23: Knee-ankle velocity trajectory tracking. $\tau_h = 0$ *(Case 3)*.

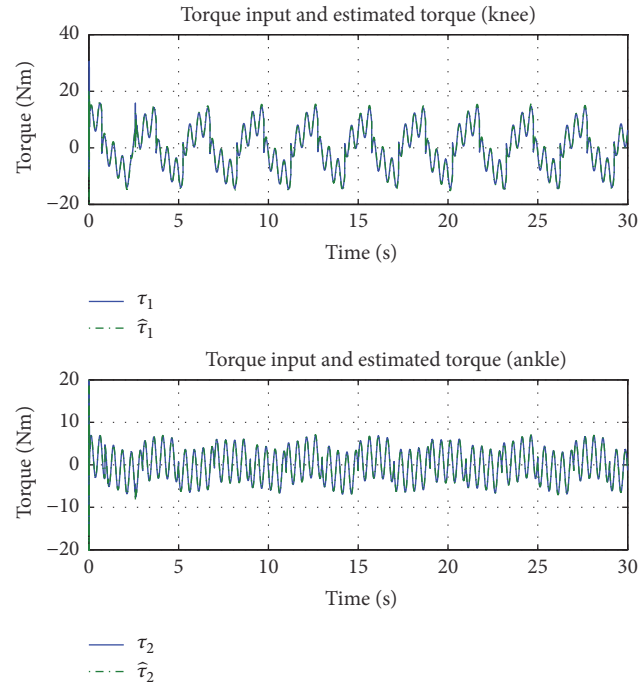

FIGURE 24: Knee-ankle torque input and estimated torque. $\tau_h = 0$. This is to exemplify a complete motor function disorder when the wearer is completely passive. The estimated torque is plotted to show that the observer can correctly estimate the exoskeleton state; hence the torque can be reconstructed *(Case 3)*.

References

[1] B. Dellon and Y. Matsuoka, "Prosthetics, exoskeletons, and rehabilitation [Grand challenges of robotics]," *IEEE Robotics and Automation Magazine*, vol. 14, no. 1, pp. 30–34, 2007.

[2] A. M. Dollar and H. Herr, "Lower extremity exoskeletons and active orthoses: challenges and state-of-the-art," *IEEE Transactions on Robotics*, vol. 24, no. 1, pp. 144–158, 2008.

[3] S. Hesse, H. Schmidt, C. Werner, and A. Bardeleben, "Upper and lower extremity robotic devices for rehabilitation and for studying motor control," *Current Opinion in Neurology*, vol. 16, no. 6, pp. 705–710, 2003.

[4] J. Hope and A. McDaid, "Development of Wearable Wrist and Forearm Exoskeleton with Shape Memory Alloy Actuators," *Journal of Intelligent & Robotic Systems*, vol. 86, no. 3-4, pp. 397–417, 2017.

[5] A. Alamdari and V. Krovi, "Design and analysis of a cable-driven articulated rehabilitation system for gait training," *Journal of Mechanisms and Robotics*, vol. 8, no. 5, Article ID 051018, 2016.

[6] K. Xu, J. Zhao, D. Qiu, and Y. Wang, "A pilot study of a continuum shoulder exoskeleton for anatomy adaptive assistances," *Journal of Mechanisms and Robotics*, vol. 6, no. 4, Article ID 041011, 2014.

[7] N. Jarrassé and G. Morel, "Connecting a human limb to an exoskeleton," *IEEE Transactions on Robotics*, vol. 28, no. 3, pp. 697–709, 2012.

[8] M. K. Vukobratovic, "When were active exoskeletons actually born?" *International Journal of Humanoid Robotics*, vol. 4, no. 3, pp. 459–486, 2007.

[9] E. Guglielmelli, M. J. Johnson, and T. Shibata, "Guest editorial: special issue on rehabilitation robotics," *IEEE Transactions on Robotics*, vol. 25, no. 3, pp. 477–480, 2009.

[10] K. P. Westlake and C. Patten, "Pilot study of Lokomat versus manual-assisted treadmill training for locomotor recovery post-stroke," *Journal of NeuroEngineering and Rehabilitation*, vol. 6, no. 1, article 18, 2009.

[11] M. H. Rahman, M. Saad, J.-P. Kenné, and P. S. Archambault, "Control of an exoskeleton robot arm with sliding mode exponential reaching law," *International Journal of Control, Automation, and Systems*, vol. 11, no. 1, pp. 92–104, 2013.

[12] N. Hogan, H. I. Krebs, B. Rohrer et al., "Motions or muscles? Some behavioral factors underlying robotic assistance of motor recovery," *Journal of Rehabilitation Research & Development*, vol. 43, no. 5, pp. 605–618, 2006.

[13] L. L. Cai, A. J. Fong, C. K. Otoshi et al., "Implications of assist-as-needed robotic step training after a complete spinal cord injury on intrinsic strategies of motor learning," *The Journal of Neuroscience*, vol. 26, no. 41, pp. 10564–10568, 2006.

[14] H. Vallery, E. H. F. Van Asseldonk, M. Buss, and H. Van Der Kooij, "Reference trajectory generation for rehabilitation robots: Complementary limb motion estimation," *IEEE Transactions on Neural Systems and Rehabilitation Engineering*, vol. 17, no. 1, pp. 23–30, 2009.

[15] K. Kong and M. Tomizuka, "Design of a rehabilitation device based on a mechanical link system," *Journal of Mechanisms and Robotics*, vol. 4, no. 3, Article ID 035001, 2012.

[16] D. G. Caldwell, N. G. Tsagarakis, S. Kousidou, N. Costa, and I. Sarakoglou, "Soft exoskeletons for upper and lower body rehabilitation - design, control and testing," *International Journal of Humanoid Robotics*, vol. 4, no. 3, pp. 549–573, 2007.

[17] K. Kiguchi, K. Iwami, M. Yasuda, K. Watanabe, and T. Fukuda, "An exoskeletal robot for human shoulder joint motion assist," *IEEE/ASME Transactions on Mechatronics*, vol. 8, no. 1, pp. 125–135, 2003.

[18] G. S. Sawicki and D. P. Ferris, "Powered ankle exoskeletons reveal the metabolic cost of plantar flexor mechanical work during walking with longer steps at constant step frequency," *Journal of Experimental Biology*, vol. 212, no. 1, pp. 21–31, 2009.

[19] C. Lintzen, Oscillator-based walking assistance.

[20] D. M. Ka, C. Hong, T. H. Toan, and J. Qiu, "Minimizing human-exoskeleton interaction force by using global fast sliding mode control," *International Journal of Control, Automation, and Systems*, vol. 14, no. 4, pp. 1064–1073, 2016.

[21] D. P. Ferris, G. S. Sawicki, and M. A. Daley, "A physiologist's perspective on robotic exoskeletons for human locomotion," *International Journal of Humanoid Robotics*, vol. 4, no. 3, pp. 507–528, 2007.

[22] J. F. Guerrero-Castellanos, N. Marchand, A. Hably, S. Lesecq, and J. Delamare, "Bounded attitude control of rigid bodies: real-time experimentation to a quadrotor mini-helicopter," *Control Engineering Practice*, vol. 19, no. 8, pp. 790–797, 2011.

[23] A. Zavala-Río and V. Santibáñez, "A natural saturating extension of the PD-with-desired-gravity-compensation control law for robot manipulators with bounded inputs," *IEEE Transactions on Robotics*, vol. 23, no. 2, pp. 386–391, 2007.

[24] Z. Flikop, "Stopping power of hot QCD plasma," *PHYSICAL REVIEW D*, 2005.

[25] H. Rifaï, W. Hassani, S. Mohammed, and Y. Amirat, "Bounded control of an actuated lower limb orthosis," in *Proceedings of the 2011 50th IEEE Conference on Decision and Control and European Control Conference, CDC-ECC 2011*, pp. 873–878, December 2011.

[26] M. O. Ajayi, K. Djouani, and Y. Hamam, "Bounded control of a full-exoskeleton device with four (4) Degree of Freedom," in *Proceedings of the IEEE International Conference on Robotics and Biomimetics, (IEEE-ROBIO '15)*, pp. 2425–2430, December 2015.

[27] A. Bateman and Z. Lin, "An analysis and design method for linear systems under nested saturation," *Systems & Control Letters*, vol. 48, no. 1, pp. 41–52, 2003.

[28] H.-B. Kang and J.-H. Wang, "Adaptive robust control of 5 DOF Upper-limb exoskeleton robot," *International Journal of Control, Automation, and Systems*, vol. 13, no. 3, pp. 733–741, 2015.

[29] Q. Van Tran, S. Kim, K. Lee, S. Kang, and J. Ryu, "Force/torque sensorless impedance control for indirect driven robot-aided gait rehabilitation system," in *Proceedings of the IEEE/ASME International Conference on Advanced Intelligent Mechatronics, AIM 2015*, pp. 652–657, July 2015.

[30] S. Oh, K. Kong, and Y. Hori, "Design and analysis of force-sensor-less power-assist control," *IEEE Transactions on Industrial Electronics*, vol. 61, no. 2, pp. 985–993, 2014.

[31] B. Ugurlu, M. Nishimura, K. Hyodo, M. Kawanishi, and T. Narikiyo, "Proof of concept for robot-aided upper limb rehabilitation using disturbance observers," *IEEE Transactions on Human-Machine Systems*, vol. 45, no. 1, pp. 110–118, 2015.

[32] G. Wang, *Observer-based feedback control methods for an underactuated robot system [Ph.D. thesis]*, Theses (School of Engineering Science)/Simon Fraser University, 2003.

[33] M. O. Ajayi, K. Djouani, and Y. Hamam, "Shank-foot trajectory control: A forward dynamics approach using computed-torque control," in *Proceedings of the 2014 14th IEEE-RAS International Conference on Humanoid Robots, Humanoids 2014*, pp. 652–657, November 2014.

[34] D. Sanz-Merodio, M. Cestari, J. C. Arevalo, X. A. Carrillo, and E. Garcia, "Generation and control of adaptive gaits in lower-limb exoskeletons for motion assistance," *Advanced Robotics*, vol. 28, no. 5, pp. 329–338, 2014.

[35] K. Radkhah, C. Maufroy, M. Maus, D. Scholz, A. Seyfarth, and O. Von Stryk, "Concept and design of the biobiped1 robot for human-like walking and running," *International Journal of Humanoid Robotics*, vol. 8, no. 3, pp. 439–458, 2011.

[36] M. Mistry, J. Buchli, and S. Schaal, "Inverse dynamics control of floating base systems using orthogonal decomposition," in *Proceedings of the 2010 IEEE International Conference on Robotics and Automation, ICRA 2010*, pp. 3406–3412, May 2010.

[37] J. L. Pons, *Wearable Robots: Biomechatronic Exoskeletons*, John Wiley & Sons, 2008.

[38] F. L. Lewis, D. M. Dawson, and C. T. Abdallah, *Robot Manipulator Control: Theory and Practice*, CRC Press, 2003.

[39] C. Souit, D. Santana Coelho, M. Szylit, F. Camargo-Junior, M. Peres Cortez Junior, and A. Forner-Cordero, "Design of a lower limb exoskeleton for experimental research on gait control," in *Proceedings of the 6th IEEE RAS/EMBS International Conference on Biomedical Robotics and Biomechatronics, BioRob 2016*, pp. 1098–1103, June 2016.

[40] D. A. Winter, *Biomechanics and Motor Control of Human Movement*, John Wiley & Sons, 2009.